ISSN 1674-1056
http://cpb.iphy.ac.cn
http://iopscience.iop.org/cpb
中国物理 B
Chinese Physics
中国物理
Chinese Physics B

The magneto-thermoelectric effect of graphene with intra-valley scattering

Wenye Duan(段文晔), Junfeng Liu(刘军丰), Chao Zhang(张潮), Zhongshui Ma(马中水)

Citation: Chin. Phys. B . 2018, 27(9): 097204. **doi:** 10.1088/1674-1056/27/9/097204

Journal homepage: http://cpb.iphy.ac.cn; http://iopscience.iop.org/cpb

What follows is a list of articles you may be interested in

Electro-statically controllable graphene local heater

Hui-Shan Wang(王慧山), Lian-Wen Deng(邓联文), Lei Li(李蕾), Qiu-Juan Sun(孙秋娟), Hong Xie(谢红), Hao-Min Wang(王浩敏)

Chin. Phys. B . 2018, 27(3): 037203. **doi:** 10.1088/1674-1056/27/3/037203

Transport properties in monolayer-bilayer-monolayer graphene planar junctions

Kai-Long Chu(储开龙), Zi-Bo Wang(王孜博), Jiao-Jiao Zhou(周娇娇), Hua Jiang(江华)

Chin. Phys. B . 2017, 26(6): 067202. **doi:** 10.1088/1674-1056/26/6/067202

High temperature characteristics of bilayer epitaxial graphene field-effect transistors on SiC Substrate

Ze-Zhao He(何泽召), Ke-Wu Yang(杨克武), Cui Yu(蔚翠), Qing-Bin Liu(刘庆彬), Jing-Jing Wang(王晶晶), Jia Li(李佳), Wei-Li Lu(芦伟立), Zhi-Hong Feng(冯志红), Shu-Jun Cai(蔡树军)

Chin. Phys. B . 2016, 25(6): 067206. **doi:** 10.1088/1674-1056/25/6/067206

A self-powered sensitive ultraviolet photodetector based on epitaxial graphene on silicon carbide

Jiao Huang(黄郊), Li-Wei Guo(郭丽伟), Wei Lu(芦伟), Yong-Hui Zhang(张永晖), Zhe Shi(史哲), Yu-Ping Jia(贾玉萍), Zhi-Lin Li(李治林), Jun-Wei Yang(杨军伟), Hong-Xiang Chen(陈洪祥), Zeng-Xia Mei(梅增霞), Xiao-Long Chen(陈小龙)

Chin. Phys. B . 2016, 25(6): 067205. **doi:** 10.1088/1674-1056/25/6/067205

Tunneling magnetoresistance based on a Cr/graphene/Cr magnetotunnel junction

Luan Gui-Ping, Zhang Pei-Ran, Jiao Na, Sun Li-Zhong

Chin. Phys. B . 2015, 24(11): 117201. **doi:** 10.1088/1674-1056/24/11/117201

The magneto-thermoelectric effect of graphene with intra-valley scattering*

Wenye Duan(段文晔)[1,2,†], Junfeng Liu(刘军丰)[3], Chao Zhang(张潮)[2], and Zhongshui Ma(马中水)[1,4]

[1] School of Physics, Peking University, Beijing 100871, China
[2] School of Physics, University of Wollongong, New South Wales 2522, Australia
[3] Department of Physics, South University of Science and Technology of China, Shenzhen 518055, China
[4] Collaborative Innovation Center of Quantum Matter, Beijing 100871, China

(Received 12 May 2018; revised manuscript received 25 June 2018; published online 28 August 2018)

We present a qualitative and quantitative study of the magneto-thermoelectric effect of graphene. In the limit of impurity scattering length being much longer than the lattice constant, the intra-valley scattering dominates the charge and thermal transport. The self-energy and the Green's functions are calculated in the self-consistent Born approximation. It is found that the longitudinal thermal conductivity splits into double peaks at high Landau levels and exhibits oscillations which are out of phase with the electric conductivity. The chemical potential-dependent electrical resistivity, the thermal conductivities, the Seebeck coefficient, and the Nernst coefficient are obtained. The results are in good agreement with the experimental observations.

Keywords: graphene, thermoelectric transport, thermal transport

PACS: 72.80.Vp, 72.15.Jf, 73.50.Lw **DOI:** 10.1088/1674-1056/27/9/097204

1. Introduction

Graphene, a single-atom-thick honeycomb-like allotrope of carbon, has attracted intense interest since it was discovered in 2004.[1] On the basis of its potential applications in electronic devices, the electromagnetic responses in graphene have been investigated. Its peculiar band structure, described by the effective massless Dirac Hamiltonian at low-energy,[2–5] results in many novel features in the electrical transport under magnetic field.[6–14] It has been shown that graphene has many unusual thermoelectric and thermal transport properties.[15–38] Because of the sensitivity to the ambipolar behavior of graphene, the measurement of thermoelectric transport properties is regarded as an effective tool to deal with the additional characteristics of graphene, which are difficult to obtain from the electric conducting measurements. The Seebeck coefficient and Nernst signal in graphene have been measured in the quantum Hall (QH) regime,[15–21] in which the Seebeck coefficient displays a large peak and the Nernst signal displays a large oscillation at each Landau level (LL). The measurement of the Seebeck coefficient exhibits an abnormal sign change around the zeroth LL in comparison with other LLs.[15–17,19] Later, extensions of the intrinsic thermal properties have been made towards the investigations of the thermoelectric effect in bilayer graphene.[39–41] There have been several theories put forward to explain the Seebeck and Nernst effects of graphene in the QH regime.[42–50] Some of the observed thermoelectric properties are not yet fully understood.

In this work, we perform a systematic study on the thermoelectric effect and thermal transport in the magnetically quantized graphene. We consider the scattering range of impurity to be much smaller than the electron wavelength and much longer than the lattice constant. In this limit, the inter-valley scattering is much weaker than the intra-valley scattering. By employing the self-consistent Born approximation (SCBA), the Green's function and the self-energy are determined. Based on the Green's functions, all other coefficients of electrical, thermoelectrical, and thermal transport are calculated within the linear response theory. Although the thermal transport properties may be influenced by the acoustic and the optical phonons through inelastic electron–phonon scattering at high temperature, the electric contribution of graphene dominates over the phonon contribution at low temperatures. The temperature in the experiments has been confirmed below 50 K.[51–53] Therefore, we neglect the effect of phonon on the graphene and concentrate on the influence of the impurity scattering in this work. The calculated results are in good agreement with the experimental findings.

The article is organized as follows. In the next section, we present the Hamiltonian describing the electrons under a strong magnetic field. The intra-valley interaction potential for the impurity scattering is introduced. The Green's function with a self-energy correction from the intra-valley impurity scattering is calculated within the SCBA. In Section 3, we present the general relations between the thermoelectric trans-

*Project supported by the National Natural Science Foundation of China (Grant Nos. 11274013 and 11774006), the National Basic Research Program of China (2012CB921300), and the Australian Research Council Grant (Grant No. DP160101474).

†Corresponding author. E-mail: duanwy@pku.edu.cn

© 2018 Chinese Physical Society and IOP Publishing Ltd

port coefficients. In Section 4, we calculate the thermoelectric response coefficients. The results are compared with the experimental measurements. A summary is given in Section 5.

2. Hamiltonian and Green's function in SCBA

2.1. Graphene in presence of a magnetic field

Utilizing the $\boldsymbol{k}\cdot\boldsymbol{p}$ method or with the effective-mass approximation,[54–58] the nearest-neighbor tight-binding model of graphene without the impurity scattering leads to an effective Hamiltonian

$$\mathcal{H}_0 = v_{\rm F}(\tau_0\otimes\sigma_x p_x + \tau_z\otimes\sigma_y p_y), \tag{1}$$

where $v_{\rm F}$ is the Fermi velocity. In this expression, σ_x, σ_y, and σ_z are the Pauli matrices describing the pseudo spins, τ_x, τ_y, and τ_z are the Pauli matrices describing the valleys $\boldsymbol{K}$ and $\boldsymbol{K}'$ in the reciprocal space, and σ_0 and τ_0 are 2×2 identity matrices. In the presence of a uniform magnetic field in the direction perpendicular to the graphene sheet, $\boldsymbol{p}$ is replaced by the mechanical momentum $\boldsymbol{\pi}=\boldsymbol{p}+e\boldsymbol{A}$. In the Landau gauge, the vector potential takes the form $\boldsymbol{A}=(0,Bx,0)$ (we use the SI units and electron charge is $-e$ ($e>0$)). We shall neglect the Zeeman energy since it is much smaller than the LL spacing. The wave function should be written in a basis

$$\Psi = (\psi_{A\boldsymbol{K}}, \psi_{B\boldsymbol{K}}, \psi_{A\boldsymbol{K}'}, -\psi_{B\boldsymbol{K}'})^{\mathcal{T}}, \tag{2}$$

where $\mathcal{T}$ stands for the transpose, $\psi_{(A/B)(\boldsymbol{K}/\boldsymbol{K}')}$ are the components of the spinors, and A and B represent the two inequivalent carbon atoms in the honeycomb hexagon lattice of graphene. The states can be obtained by solving the eigen equation $\mathcal{H}_0\Psi=\varepsilon\Psi$. The eigenvalues are

$$\varepsilon_n = \mathrm{sgn}(n)\,\hbar\omega\sqrt{|n|}, \tag{3}$$

and the eigenstates are given by $\Psi^{\eta}_{n,k_y}(x,y) = C_n\left(1/\sqrt{L_y}\right)\mathrm{e}^{\mathrm{i}k_y y}\Phi^{\eta}_{n,k_y}(x)$, with

$$\Phi^{+}_{n,k_y}(x) = \left(-\mathrm{isgn}(n)\,\phi_{|n|-1,k_y}(x), \phi_{|n|,k_y}(x), 0, 0\right)^{\mathcal{T}}, \tag{4}$$

$$\Phi^{-}_{n,k_y}(x) = \left(0, 0, \phi_{|n|,k_y}(x), -\mathrm{isgn}(n)\,\phi_{|n|-1,k_y}(x)\right)^{\mathcal{T}}, \tag{5}$$

where $C_n=1$ for $n=0$ and $1/\sqrt{2}$ for $n\neq 0$, $\mathrm{sgn}(x)$ is the sign function,

$$\phi_{|n|,k_y}(x) = \frac{\exp\left[-\frac{1}{2}\left(\frac{x+k_y l^2}{l}\right)^2\right]}{\left(2^{|n|}\,|n|!\sqrt{\pi}l\right)^{1/2}}\mathrm{H}_{|n|}\left(\frac{x+k_y l^2}{l}\right),$$

n is an integer number, $\mathrm{H}_n(x)$ is the Hermite polynomial, k_y is the wave vector along the y direction, $l=\sqrt{\hbar/eB}$, $\hbar\omega=\sqrt{2}\hbar v_{\rm F}/l$, and $\eta=\pm 1$ for the $\boldsymbol{K}(+)$ and $\boldsymbol{K}'(-)$ valleys, respectively.

2.2. Intra-valley impurity scattering

Now we consider the impurity scattering. Utilizing the $\boldsymbol{k}\cdot\boldsymbol{p}$ method or with the effective-mass approximation,[54–60] the effective potential with impurity scatters at $\boldsymbol{r}_i^{\zeta}$ ($\zeta=A,B$) is given by

$$U(\boldsymbol{r}) = \sum_{\zeta,\boldsymbol{r}_i^{\zeta}}\begin{pmatrix} u_A(\boldsymbol{r}-\boldsymbol{r}_i^{\zeta}) & 0 & u'_A(\boldsymbol{r}-\boldsymbol{r}_i^{A})\mathrm{e}^{\mathrm{i}\theta_i^A} & 0 \\ 0 & u_B(\boldsymbol{r}-\boldsymbol{r}_i^{\zeta}) & 0 & u'_B(\boldsymbol{r}-\boldsymbol{r}_i^{B})\mathrm{e}^{\mathrm{i}\theta_i^B} \\ u'^{*}_A(\boldsymbol{r}-\boldsymbol{r}_i^{A})\mathrm{e}^{-\mathrm{i}\theta_i^A} & 0 & u_A(\boldsymbol{r}-\boldsymbol{r}_i^{\zeta}) & 0 \\ 0 & u'^{*}_B(\boldsymbol{r}-\boldsymbol{r}_i^{B})\mathrm{e}^{-\mathrm{i}\theta_i^B} & 0 & u_B(\boldsymbol{r}-\boldsymbol{r}_i^{\zeta}) \end{pmatrix}, \tag{6}$$

where $\theta_i^{\zeta}=(\boldsymbol{K}'-\boldsymbol{K})\cdot\boldsymbol{r}_i^{\zeta}$. If the effective range of the impurity potential is much smaller than the typical electron wavelength, (which is the case near the Dirac point), the $\boldsymbol{r}$-dependent potentials can be approximated by $\delta(\boldsymbol{r}-\boldsymbol{r}_i)$. On the other hand, if the effective range of the impurity potential is larger than the lattice constant, the inter-valley scattering between $\boldsymbol{K}$ and $\boldsymbol{K}'$ valleys can be neglected.[56,58–60] This argument was used to classify the intra-valley potentials as types of long-range potentials by Ando *et al.*[56,60] The scattering potential is written as

$$U_i(\boldsymbol{r}) = \tau_0\otimes\sigma_0 u_i\delta(\boldsymbol{r}-\boldsymbol{r}_i), \tag{7}$$

where $\boldsymbol{r}_i$ is the impurity position and u_i is the intensity of the scattering. The intra-valley scattering forbids the scattering between the states in $\boldsymbol{K}$ and $\boldsymbol{K}'$ points. Including the scattering potential in Eq. (7), the full Hamiltonian is given by $\mathcal{H}=\mathcal{H}_0+U(\boldsymbol{r})$, where $U(\boldsymbol{r})=\sum_i U_i(\boldsymbol{r})$.

2.3. Green's function with the self-energy corrections in SCBA

The Green's function is defined by $G(\varepsilon)=[\varepsilon-\mathcal{H}]^{-1}$. The matrix elements of the unperturbed Green's function in the representation of the LL basis are diagonal, i.e., $G^{(0)}_{\alpha\alpha'}(\varepsilon)=\langle\alpha|[\varepsilon-\mathcal{H}_0]^{-1}|\alpha'\rangle=\delta_{\alpha\alpha'}G^{(0)}_{\alpha}(\varepsilon)$, where

$$G^{(0)}_{\alpha}(\varepsilon) = \frac{1}{\varepsilon-\mathrm{sgn}(n)\,\hbar\omega\sqrt{|n|}}, \tag{8}$$

specified in a set of quantum numbers $\alpha=(\eta,n,k_y)$.

The electron–impurity scattering is studied through the impurity-averaged Green's function within the SCBA. The disorder term Eq. (7) is treated perturbatively with respect to

the impurity-free Green's function $G_{\alpha}^{(0)}(\varepsilon)$. Averaging over all possible configurations of random distributions of impurities, the matrix elements of $G(\varepsilon)$ are given by Dyson's equation

$$\begin{aligned}\langle G_{\alpha\alpha'}(\varepsilon)\rangle &= \delta_{\alpha\alpha'}G_{\alpha}^{(0)}(\varepsilon)\\ &\quad +G_{\alpha}^{(0)}(\varepsilon)\sum_{\alpha'}\Sigma_{\alpha\alpha'}(\varepsilon)\langle G_{\alpha\alpha'}(\varepsilon)\rangle,\end{aligned}\tag{9}$$

where the self-energy $\Sigma_{\alpha\alpha'}(\varepsilon)$ is introduced within the SCBA,

$$\Sigma_{\alpha\alpha'}(\varepsilon)=\sum_{\alpha_1\alpha_1'}\left\langle U_{\alpha\alpha_1}U_{\alpha_1'\alpha'}(\varepsilon)\right\rangle\left\langle G_{\alpha_1\alpha_1'}(\varepsilon)\right\rangle,\tag{10}$$

and $G(\varepsilon)=[\varepsilon-\mathcal{H}_0-\Sigma(\varepsilon)]^{-1}$. The average Green's function and the self-energy can be derived self-consistently for random impurities $\left\langle(u_i)^2\right\rangle=u^2$. The concentration of impurities is given by $n_{\rm im}$. The self-energy can be decomposed into a diagonal part $\bar{\Sigma}^{(\rm D)}(\varepsilon)$ and an off-diagonal part $\bar{\Sigma}^{(\rm O)}(\varepsilon)$, i.e.,

$$\Sigma_{\alpha\alpha'}(\varepsilon)=\delta_{\alpha\alpha'}\bar{\Sigma}^{(\rm D)}(\varepsilon)+\delta_{\alpha,-\alpha'}\bar{\Sigma}^{(\rm O)}(\varepsilon),\tag{11}$$

where $\pm\alpha=(\eta,\pm n,k_y)$ is a composite quantum number. The off-diagonal elements between the LL indices $+n$ and $-n$ are non vanishing. The self-energy terms in the above equation can be written as

$$\bar{\Sigma}^{(\rm D)}(\varepsilon)=\frac{V}{2}(\hbar\omega)^2\sum_{n=-N_{\rm c}}^{N_{\rm c}}\left[\bar{G}_n^{(\rm D)}(\varepsilon)+\bar{G}_0^{(\rm O)}(\varepsilon)\right],\tag{12}$$

$$\bar{\Sigma}^{(\rm O)}(\varepsilon)=\frac{V}{2}(\hbar\omega)^2\sum_{n=-N_{\rm c}}^{N_{\rm c}}\left[\bar{G}_n^{(\rm O)}(\varepsilon)+\bar{G}_0^{(\rm D)}(\varepsilon)\right],\tag{13}$$

where the dimensionless parameter $V=n_{\rm im}u^2/\left(4\pi v_{\rm F}^2\right)$ is a measure of the intensity of scattering within the SCBA.

The impurity-averaged Green's functions are reduced to the form

$$\langle G_{\alpha\alpha'}(\varepsilon)\rangle=\delta_{\alpha\alpha'}\bar{G}_n^{(\rm D)}(\varepsilon)+\delta_{\alpha,-\alpha'}\bar{G}_n^{(\rm O)}(\varepsilon),\tag{14}$$

where

$$\bar{G}_n^{(\rm D)}(\varepsilon)=\frac{\varepsilon+\varepsilon_n-\bar{\Sigma}^{(\rm D)}}{\left(\varepsilon+\varepsilon_n-\bar{\Sigma}^{(\rm D)}\right)\left(\varepsilon-\varepsilon_n-\bar{\Sigma}^{(\rm D)}\right)-\left(\bar{\Sigma}^{(\rm O)}\right)^2},\tag{15}$$

$$\bar{G}_n^{(\rm O)}(\varepsilon)=\frac{\bar{\Sigma}^{(\rm O)}}{\left(\varepsilon+\varepsilon_n-\bar{\Sigma}^{(\rm D)}\right)\left(\varepsilon-\varepsilon_n-\bar{\Sigma}^{(\rm D)}\right)-\left(\bar{\Sigma}^{(\rm O)}\right)^2}.\tag{16}$$

The scattering matrix elements between different quantum states are given by

$$\begin{aligned}&U_{nn',k_yk_y',\eta\eta'}\\ &=u_i\delta_{q_y,k_y-k_y'}\delta_{\eta\eta'}{\rm e}^{-{\rm i}\boldsymbol{q}\cdot\boldsymbol{r}_i}C_nC_{n'}{\rm sgn}(n)\,{\rm sgn}\left(n'\right)\\ &\quad\times\left[I_{|n|,|n'|}+I_{|n|-1,|n'|-1}\right],\end{aligned}\tag{17}$$

where

$$\begin{aligned}I_{|n|,|n'|}&=(-1)^{\frac{M-N}{2}}\frac{N!\left(\frac{q_xl}{\sqrt{2}}\right)^{M-N}{\rm L}_N^{(M-N)}\left(\left(\frac{q_xl}{\sqrt{2}}\right)^2\right)}{\sqrt{(|n|-1)!}\sqrt{(|n'|-1)!}}\\ &\quad\times\exp\left[\frac{q_xl}{4}({\rm i}4lk_y-q_xl)\right],\end{aligned}$$

$N=\min(|n|-1,|n'|-1)$, $M=\max(|n|-1,|n'|-1)$, and ${\rm L}_N^{(M-N)}(x)$ is the associated Laguerre polynomial.

3. Linear response theory and transport coefficients

Within the linear response theory, under an applied field and a temperature gradient, the electrical current $\boldsymbol{j}^C$ and energy current $\boldsymbol{j}^E$ can be written in the general form

$$\boldsymbol{j}^C=\mathbb{L}^{CC}\cdot\boldsymbol{E}+\mathbb{L}^{CE}\cdot\boldsymbol{X}^E,\tag{18}$$

$$\boldsymbol{j}^E=\mathbb{L}^{EC}\cdot\boldsymbol{E}+\mathbb{L}^{EE}\cdot\boldsymbol{X}^E,\tag{19}$$

where the external force for the temperature gradient is expressed in the form $\boldsymbol{X}^E=T\boldsymbol{\nabla}(1/T)$. The coefficients $\mathbb{L}^{CC}$, $\mathbb{L}^{CE}$, $\mathbb{L}^{EC}$, and $\mathbb{L}^{EE}$ are general tensors. They can be expressed in terms of the current–current correlations $\mathbb{N}^{ij}$ together with the corrections from the magnetization $\mathbb{M}^{ij}$, $\mathbb{L}^{ij}=\mathbb{N}^{ij}+\mathbb{M}^{ij}$,[61–64] with the subscripts i and j ($=C$ or E) standing for the charge and the energy currents in the current–current correlations. Utilizing the Kubo–Středa formalism, the current–current correlation $\mathbb{N}^{ij}$ is given by

$$\begin{aligned}\mathbb{N}_{ab}^{ij}(T,\mu)&=\frac{{\rm i}\hbar}{L^2}\int_{-\infty}^{+\infty}{\rm d}\varepsilon f_{\rm F}(\varepsilon){\rm Tr}\Bigg\langle\Bigg[J_a^i\frac{{\rm d}G(\varepsilon_{+0})}{{\rm d}\varepsilon}J_b^j\delta(\varepsilon-\mathcal{H})\\ &\quad-J_a^i\delta(\varepsilon-\mathcal{H})J_b^j\frac{{\rm d}G(\varepsilon_{-0})}{{\rm d}\varepsilon}\Bigg]\Bigg\rangle,\end{aligned}\tag{20}$$

while the corrections due to the magnetization $\mathbb{M}_{ij}$ are $\mathbb{M}_{CC}^{ab}=0$,

$$\mathbb{M}_{ab}^{CE}=-\frac{e}{2L^2}\int_{-\infty}^{+\infty}{\rm d}\varepsilon f_{\rm F}(\varepsilon){\rm Tr}\left\langle[\delta(\varepsilon-\mathcal{H})(r_av_b-r_bv_a)]\right\rangle,\tag{21}$$

$$\mathbb{M}_{ab}^{EE}=\frac{1}{L^2}\int_{-\infty}^{+\infty}{\rm d}\varepsilon f_{\rm F}(\varepsilon){\rm Tr}\left\langle[\delta(\varepsilon-\mathcal{H})\mathcal{H}(r_av_b-r_bv_a)]\right\rangle,\tag{22}$$

where a and b denote the spatial components (x or y), $\varepsilon_{\pm0}=\varepsilon\pm{\rm i}0$, J_a^C ($=-ev_a$) and J_a^E ($=\{\mathcal{H},v_a\}/2$) are the operators of charge current and energy flux, respectively, $f_{\rm F}(\varepsilon)=1/(1+{\rm e}^{(\varepsilon-\mu)/k_{\rm B}T})$ is the equilibrium Fermi–Dirac distribution function, L^2 is the area of the system, and the velocity operators $\boldsymbol{v}=(-{\rm i}/\hbar)[\boldsymbol{r},\mathcal{H}]$. The physical meanings of the coefficients in Eqs. (18) and (19) are as follows: $\mathbb{L}^{CC}=\boldsymbol{\sigma}$ is the electrical conductivity, $(1/T)\left[(\mu/e)+\mathbb{L}^{CC-1}\cdot\mathbb{L}^{CE}\right]=\boldsymbol{S}$ is the thermopower, $(1/T)\left[\mathbb{L}^{EE}-\mathbb{L}^{EC}\cdot\mathbb{L}^{CC-1}\cdot\mathbb{L}^{CE}\right]=\boldsymbol{\kappa}$ is the thermal conductivity, and the thermoelectric figure of merit $ZT=\sigma_{xx}S_{xx}^2T/\kappa_{xx}$. The thermopower and the thermal conductivity are obtained under the condition of zero electric current.

The electrical conductivity is given by $\sigma_{ab}(T,\mu)=L_{ab}^{CC}(T,\mu)$ and can be written in the form

$$\sigma_{ab}(T,\mu)=\sigma_{ab}^{\rm I}(T,\mu)+\sigma_{ab}^{\rm II}(T,\mu).\tag{23}$$

$\sigma^{\rm I}_{ab}(T,\mu)$ and $\sigma^{\rm II}_{ab}(T,\mu)$ can be obtained from the Green's functions by the following formula:

$$\sigma^{\rm I}_{ab}(T,\mu) = \int_{-\infty}^{+\infty} {\rm d}\varepsilon \left[-\frac{{\rm d}f_{\rm F}(\varepsilon)}{{\rm d}\varepsilon}\right] \sigma^{\rm I}_{ab}(0,\mu), \tag{24}$$

$$\sigma^{\rm II}_{ab}(T,\mu) = \frac{g_{\rm s}e^2\hbar}{4\pi L^2}\int_{-\infty}^{+\infty} {\rm d}\varepsilon f_{\rm F}(\varepsilon) {\rm Tr}\Big\langle v_a \frac{{\rm d}G(\varepsilon_{-0})}{{\rm d}\varepsilon} v_b G(\varepsilon_{-0}) - v_a \frac{{\rm d}G(\varepsilon_{+0})}{{\rm d}\varepsilon} v_b G(\varepsilon_{+0}) - (a\leftrightarrow b)\Big\rangle, \tag{25}$$

where

$$\sigma^{\rm I}_{ab}(0,\varepsilon) = \frac{g_{\rm s}e^2\hbar}{4\pi L^2}{\rm Tr}\big\langle v_a\left(G(\varepsilon_{+0})-G(\varepsilon_{-0})\right)v_b G(\varepsilon_{-0}) - v_a G(\varepsilon_{+0})\, v_b\left(G(\varepsilon_{+0})-G(\varepsilon_{-0})\right)\big\rangle, \tag{26}$$

$g_{\rm s}$ is the degeneracy of spin. Applying the relations $\boldsymbol{v} = (-{\rm i}/\hbar)[\boldsymbol{r},\mathcal{H}]$ and ${\rm d}G(\varepsilon\pm{\rm i}0)/{\rm d}\varepsilon = -[G(\varepsilon\pm{\rm i}0)]^2$, $\sigma^{\rm II}_{ab}(T,\mu)$ can be rewritten as

$$\sigma^{\rm II}_{ab}(T,\mu) = \int_{-\infty}^{+\infty} {\rm d}\varepsilon \left[-\frac{{\rm d}f_{\rm F}(\varepsilon)}{{\rm d}\varepsilon}\right] \sigma^{\rm II}_{ab}(0,\varepsilon), \tag{27}$$

where

$$\sigma^{\rm II}_{ab}(0,\varepsilon) = -\frac{g_{\rm s}e^2}{4{\rm i}\pi L^2}{\rm Tr}\left\langle (r_a v_b - r_b v_a)\left(G(\varepsilon_{+0})-G(\varepsilon_{-0})\right)\right\rangle. \tag{28}$$

The electrical conductivity is expressed as

$$\sigma_{ab}(T,\mu) = \int {\rm d}\varepsilon \left[-\frac{{\rm d}f_{\rm F}(\varepsilon)}{{\rm d}\varepsilon}\right] \sigma_{ab}(0,\varepsilon), \tag{29}$$

with $\sigma_{ab}(0,\varepsilon) = \sigma^{\rm I}_{ab}(0,\varepsilon) + \sigma^{\rm II}_{ab}(0,\varepsilon)$. In the calculations of $\sigma_{ab}(0,\mu)$, we need to use the matrix elements of the velocity operators in the representation of the LL basis

$$v_{x,\alpha\alpha'} = v_{\rm F} C_{n'} C_n \delta_{\kappa\kappa'}\delta_{k_y k_y'}\left[{\rm isgn}(n')\delta_{|n|+1,|n'|} - {\rm isgn}(n)\delta_{|n|-1,|n'|}\right], \tag{30}$$

$$v_{y,\alpha\alpha'} = v_{\rm F} C_n C_{n'} \delta_{\kappa\kappa'}\delta_{k_y k_y'}\left[{\rm sgn}(n)\delta_{|n|-1,|n'|} + {\rm sgn}(n')\delta_{|n|+1,|n'|}\right], \tag{31}$$

and the vortex correction in the SCBA

$$\Gamma = \langle G(\varepsilon) v_a G(\varepsilon)\rangle = \langle G(\varepsilon)\rangle v_a \langle G(\varepsilon)\rangle + \langle G(\varepsilon)\rangle \langle U\Gamma U\rangle \langle G(\varepsilon)\rangle. \tag{32}$$

Similar with the conductivity, it has been shown that $\mathbb{L}^{CE}_{ab}(T,\mu)$ and $\mathbb{L}^{EE}_{ab}(T,\mu)$ can be obtained in terms of $\sigma_{ab}(0,\varepsilon)$ through the following relations:[61,63,65]

$$\mathbb{L}^{CE}_{ab}(T,\mu) = \mathbb{L}^{EC}_{ab}(T,\mu) = -\frac{1}{e}\int {\rm d}\varepsilon \left[-\frac{{\rm d}f_{\rm F}(\varepsilon)}{{\rm d}\varepsilon}\right] \varepsilon\sigma_{ab}(0,\varepsilon), \tag{33}$$

$$\mathbb{L}^{EE}_{ab}(T,\mu) = \frac{1}{e^2}\int {\rm d}\varepsilon \left[-\frac{{\rm d}f_{\rm F}(\varepsilon)}{{\rm d}\varepsilon}\right] \varepsilon^2\sigma_{ab}(0,\varepsilon). \tag{34}$$

4. The magneto-transport coefficients of graphene

The thermoelectric and thermal response coefficients can be obtained by Eqs. (29), (33), and (34). In the following subsection, we will evaluate the conductivity tensor by the Green's functions within the SCBA.

4.1. Analytical formula for calculating the conductivity

4.1.1. The longitudinal conductivity

The longitudinal conductivity is σ_{xx}. Since $(r_x v_x - r_x v_x) = 0$, therefore equation (28) shows $\sigma^{\rm II}_{xx}(0,\varepsilon) = 0$. The longitudinal conductivity is $\sigma_{xx}(T,\mu) = \sigma^{\rm I}_{xx}(T,\mu) = \int_{-\infty}^{+\infty}{\rm d}\varepsilon\left[-({\rm d}f_{\rm F}(\varepsilon)/{\rm d}\varepsilon)\right]\sigma^{\rm I}_{xx}(0,\varepsilon)$, where

$$\sigma^{\rm I}_{xx}(0,\varepsilon) = 2Y_{xx}(\varepsilon_{+0},\varepsilon_{-0}) - Y_{xx}(\varepsilon_{+0},\varepsilon_{+0}) - Y_{xx}(\varepsilon_{-0},\varepsilon_{-0}), \tag{35}$$

with

$$Y_{ab}(\varepsilon,\varepsilon') = \frac{g_{\rm s}e^2\hbar}{4\pi L^2}{\rm Tr}\left\langle v_a G(\varepsilon) v_b G(\varepsilon')\right\rangle. \tag{36}$$

Taking account of the impurity scattering within SCBA, it is found that

$$Y_{xx}(\varepsilon,\varepsilon') = \frac{g_{\rm s}e^2}{2\pi h}\sum_{\beta=1,2}\frac{\varphi^\beta(\varepsilon,\varepsilon')}{\left(1-2V\varphi^\beta(\varepsilon,\varepsilon')\right)}, \tag{37}$$

where $\varphi^1(\varepsilon,\varepsilon') = \left[(\hbar\omega)^2/2\right]\sum_{n\geq 0}\tilde{g}^-_{n+1}(\varepsilon)\tilde{g}^+_n(\varepsilon')$ and $\varphi^2(\varepsilon,\varepsilon') = \left[(\hbar\omega)^2/2\right]\sum_{n\geq 0}\tilde{g}^+_n(\varepsilon)\tilde{g}^-_{n+1}(\varepsilon')$. We define $\tilde{g}^\pm_n(\varepsilon)$ as $\tilde{g}^\pm_n(\varepsilon) \equiv (1/2)\left[\tilde{G}^\pm_n(\varepsilon) + \tilde{G}^\pm_{-n}(\varepsilon)\right]$, where $\tilde{G}^\pm_n(\varepsilon) \equiv \tilde{G}^{(\rm D)}_n(\varepsilon) \pm \tilde{G}^{(\rm O)}_n(\varepsilon)$. The self-energy can be obtained by self-consistently solving the equation

$$\tilde{\Sigma}^\pm(\varepsilon) = V(\hbar\omega)^2\sum_{n=0}^{N_{\rm c}}\frac{\varepsilon-\tilde{\Sigma}^\mp}{\left(\varepsilon-\tilde{\Sigma}^+\right)\left(\varepsilon-\tilde{\Sigma}^-\right)-\varepsilon_n^2}. \tag{38}$$

Then the Green's functions $\tilde{G}^\pm_n(\varepsilon)$ are obtained as $\tilde{G}^\pm_n(\varepsilon) = \left(\varepsilon+\varepsilon_n-\tilde{\Sigma}^\mp\right)/\left[\left(\varepsilon-\tilde{\Sigma}^+\right)\left(\varepsilon-\tilde{\Sigma}^-\right)-\varepsilon_n^2\right]$, so that $\tilde{g}^\pm_n(\varepsilon) = \left(\varepsilon-\tilde{\Sigma}^\mp\right)/\left[\left(\varepsilon-\tilde{\Sigma}^+\right)\left(\varepsilon-\tilde{\Sigma}^-\right)-\varepsilon_n^2\right]$.

4.1.2. The Hall conductivity

We now calculate the Hall conductivity σ_{xy}. $\sigma^{\rm I}_{xy}(0,\varepsilon)$ is found as

$$\sigma^{\rm I}_{xy}(0,\varepsilon) = 2Y_{xy}(\varepsilon_{+0},\varepsilon_{-0}) - Y_{xy}(\varepsilon_{+0},\varepsilon_{+0}) - Y_{xy}(\varepsilon_{-0},\varepsilon_{-0}), \tag{39}$$

where

$$Y_{xy}(\varepsilon,\varepsilon') = \frac{g_{\rm s}e^2}{2\pi h}\sum_{\beta=1,2}(-1)^{\beta+1}\frac{\varphi^\beta(\varepsilon,\varepsilon')}{\left(1-2V\varphi^\beta(\varepsilon,\varepsilon')\right)}. \tag{40}$$

We have $\sigma^{\rm I}_{xy}(T,\mu) = \int_{-\infty}^{+\infty}{\rm d}\varepsilon\left[-({\rm d}f_{\rm F}(\varepsilon)/{\rm d}\varepsilon)\right]\sigma^{\rm I}_{xy}(0,\varepsilon)$. $\sigma^{\rm II}_{xy}(0,\varepsilon)$ is found as

$$\sigma^{\rm II}_{xy}(0,\varepsilon) = \frac{g_{\rm s}e^2}{2L^2}{\rm Tr}\left\langle (r_x v_y - r_y v_x)\,\delta(\varepsilon-H)\right\rangle, \tag{41}$$

where we have used the relation $\delta(\varepsilon - H) = (\mathrm{i}/2\pi)[G(\varepsilon_{+0}) - G(\varepsilon_{-0})]$. $\sigma_{xy}^{\mathrm{II}}(T,\mu)$ can be written as

$$\sigma_{xy}^{\mathrm{II}}(T,\mu) = \frac{g_s e^2}{2L^2}\int_{-\infty}^{+\infty} \mathrm{d}\varepsilon f_{\mathrm{F}}(\varepsilon)\,\mathrm{Tr}\left\langle (r_x v_y - r_y v_x)\frac{\mathrm{d}\delta(\varepsilon - H)}{\mathrm{d}\varepsilon}\right\rangle.$$

Under the Landau gauge, we have $\boldsymbol{A} = B(0,x,0)$ for the magnetic field along the z-axis $\boldsymbol{B} = (0,0,B)$. The terms in the trace can be written in the form $(1/2)\,\mathrm{Tr}\left[(r_x v_y - r_y v_x)\,\mathrm{d}\delta(\varepsilon - \mathcal{H})/\mathrm{d}\varepsilon\right] = -(1/e)\,\partial\left[\mathrm{Tr}\delta(\varepsilon - \mathcal{H})\right]/\partial B$. $\sigma_{xy}^{\mathrm{II}}(T,\mu)$ becomes $\sigma_{xy}^{\mathrm{II}}(T,\mu) = -\left(g_s e/L^2\right)\int_{-\infty}^{+\infty}\mathrm{d}\varepsilon f_{\mathrm{F}}(\varepsilon)\quad\langle\partial\mathrm{Tr}\delta(\varepsilon - \mathcal{H})/\partial B\rangle$. Because the particle number is found as $\mathcal{N}(T,\mu) = g_s\int_{-\infty}^{+\infty}\mathrm{d}\varepsilon f_{\mathrm{F}}(\varepsilon)\,\mathrm{Tr}\delta(\varepsilon - \mathcal{H})$, $\sigma_{xy}^{\mathrm{II}}(T,\mu)$ is expressed in terms of the particle number $\sigma_{xy}^{\mathrm{II}}(T,\mu) = -\left(e/L^2\right)\left\langle(\partial\mathcal{N}(T,\mu)/\partial B)_{\mu}\right\rangle$. Utilizing the density of states $D(\varepsilon) = -\left(g_s/\pi^2 l^2\right)\sum_n \mathrm{Im}\langle G_{nn}(\varepsilon_{+0})\rangle$ and $\mathcal{N}(T,\mu) = -\left(g_s eB/\pi^2\hbar\right)\int_{-\infty}^{+\infty}\mathrm{d}\varepsilon f_{\mathrm{F}}(\varepsilon)\sum_n \mathrm{Im}\langle G_{nn}(\varepsilon_{+0})\rangle$, $\sigma_{xy}^{\mathrm{II}}(T,\mu)$ is found as

$$\sigma_{xy}^{\mathrm{II}}(T,\mu) = \frac{2g_s e^2}{\pi h}\int_{-\infty}^{+\infty}\mathrm{d}\varepsilon f_{\mathrm{F}}(\varepsilon)\sum_n \mathrm{Im}\langle G_{nn}(\varepsilon_{+0})\rangle + \frac{g_s e^2}{\pi h}\int_{-\infty}^{+\infty}\mathrm{d}\varepsilon\frac{\partial f_{\mathrm{F}}(\varepsilon)}{\partial\varepsilon}\sum_n \varepsilon_n \mathrm{Im}\langle G_{nn}(\varepsilon_{+0})\rangle. \quad (42)$$

Finally, we obtain the Hall conductivity $\sigma_{xy}(T,\mu) = \sigma_{xy}^{\mathrm{I}}(T,\mu) + \sigma_{xy}^{\mathrm{II}}(T,\mu)$.

4.2. Thermoelectric coefficients

In the following, we present the numerical results of the thermoelectric coefficients as a function of the chemical potential.

4.2.1. Resistivities ρ_{xx} and ρ_{xy}

Using Eqs. (35), (39), and (42), we can obtain the conductivities σ_{xx} and σ_{xy} numerically. The longitudinal resistivity ρ_{xx} and the Hall resistivity ρ_{xy} are obtained by using the equations $\rho_{xx} = \sigma_{xx}/\left(\sigma_{xx}^2 + \sigma_{xy}^2\right)$ and $\rho_{xy} = -\sigma_{xy}/\left(\sigma_{xx}^2 + \sigma_{xy}^2\right)$.

The longitudinal resistivity ρ_{xx} and the Hall resistivity ρ_{xy} are depicted in Fig. 1(a) with several values of V. Considering that ρ_{xx} is symmetric and ρ_{xy} is antisymmetric with respect to $\mu = 0$, only the $n \geq 0$ LLs are shown in Fig. 1(a). As expected, ρ_{xx} displays the peaks at the LLs and vanishes between each consecutive LL, while ρ_{xy} exhibits the typical Hall plateaus. The longitudinal resistivity ρ_{xx} and Hall resistivity ρ_{xy} are closely related to the localization picture in the 2D integer quantum Hall effect (IQHE), i.e., the extended states are at the center of the broadened LLs and all the other states are localized. The fluctuation of impurity scattering removes the sharpness of the LLs so that the LLs are broadened as shown in Fig. 1(a). The zeroth LL ($n = 0$), is the charge neutrality point of graphene. When the chemical potential is varied through the zeroth LL, a zero-crossing of Hall resistivity ρ_{xy} changes smoothly through zero from its negative quantized value on the hole side to a positive quantized value on the electron side, whereas ρ_{xx} moves from a zero on the hole side through a maximum at the charge neutrality point to another zero on the electron side. Our numerical results of the resistivity agree with the observations in Kim's experiment.[16] These results demonstrate that the system is in the Hall regime. The temperature dependence of the ρ_{xx} at the charge neutrality point displays an activated behavior. For the other LLs, the above picture does not change qualitatively. As the temperature increases, the peak values of ρ_{xx} decrease and the half widths increase for $n > 0$ LLs as shown in Fig. 2(a).

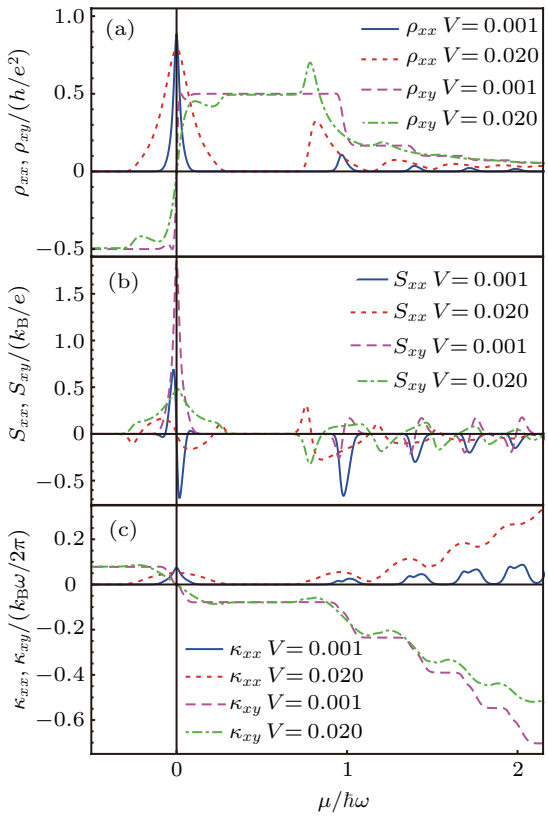


Fig. 1. (color online) (a) The longitudinal resistivity ρ_{xx} and Hall resistivity ρ_{xy}, (b) the Seebeck coefficient S_{xx} and Nernst coefficient S_{xy}, (c) the thermal conductivity κ_{xx} and thermal Hall conductivity κ_{xy} as a function of μ with different V at temperature $T = 5$ K.

4.2.2. Seebeck coefficient S_{xx} and Nernst coefficient S_{xy}

The Seebeck coefficient S_{xx} and Nernst coefficient S_{xy} are presented in Figs. 1(b) and 2(b). S_{xx} is antisymmetric and S_{xy} is symmetric with respect to $\mu = 0$. It is found that as a function of chemical potential, the Seebeck coefficient S_{xx} displays a series of peaks at the LLs for $\mu < 0$ and dips at the LLs for $\mu > 0$. $|S_{xx}|$ has a maximum while the sign of S_{xy} is alternated around the LLs ($n \geq 1$), corresponding to the extended states at the LLs. The appearance of zero thermoelectric response can be explained by the existence of the

localized states in the gap between adjacent LLs, similar to the longitudinal conductivity in the IQHE. $\boldsymbol{S}$ is defined by $\boldsymbol{\rho}\cdot\boldsymbol{\alpha}$, where $\boldsymbol{\alpha}=(1/T)[(\mu/e)\mathbb{L}_{CC}+\mathbb{L}_{CE}]$. From this, we have $S_{xx}=\rho_{xx}\alpha_{xx}-\rho_{xy}\alpha_{xy}$ and $S_{xy}=\rho_{xy}\alpha_{yy}+\rho_{xx}\alpha_{xy}$. ρ_{aa} and α_{ab} $(a\neq b)$ are symmetric functions of μ, while ρ_{ab} and α_{aa} are antisymmetric functions of μ. As the Fermi level passes through the core of extended states where the longitudinal resistance becomes appreciable and the Hall resistance makes its transition from one plateau step to the next. Their combination leads the oscillatory structure of S_{xy} in the vicinity of the LLs. As shown in Fig. 1(b), the broadening of the LLs due to the impurity scattering increases the width of the peaks or dips for Seebeck coefficient S_{xx} and oscillations of Nernst coefficients S_{xy}. As the temperature increases, S_{xx} increases and S_{xy} decreases for $n\geq 1$ LLs as shown in Fig. 2(b).

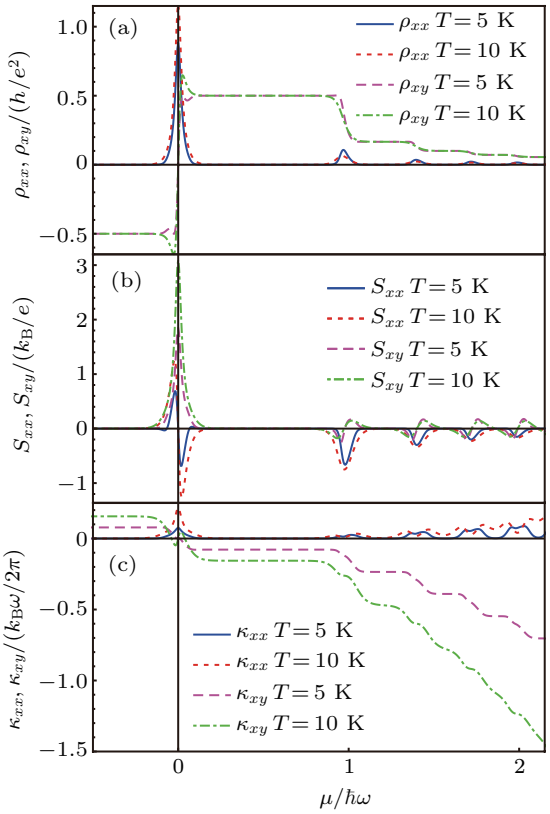


Fig. 2. (color online) (a) The longitudinal resistivity ρ_{xx} and Hall resistivity ρ_{xy}, (b) the Seebeck coefficient S_{xx} and Nernst coefficient S_{xy}, (c) the thermal conductivity κ_{xx} and thermal Hall conductivity κ_{xy} as a function of μ at different temperatures with $V=0.001$.

The Seebeck and Nernst coefficients in the vicinity of the zeroth LL have an opposite behavior compared with those in the higher LLs. Instead of S_{xx}, the Nernst coefficient S_{xy} displays a large peak while the Seebeck coefficient S_{xx} now displays an alternate sign. The feature at $n=0$ LL reflects the characteristic property of 2D relativistic fermions in the perpendicular magnetic field. Around the zeroth LL ($n=0$), the Hall resistivity changes sign because the charges have opposite signs. As in the analysis above, the Seebeck coefficient from the edge states is larger when the chemical potential is below the LL, and the resistivity for the hole-like quasiparticles makes S_{xx} negative. When the chemical potential lies near the top of the lowest LL, i.e., in the electron side, S_{xx} behaves similarly as in the higher LLs. Hence, the Seebeck coefficient S_{xx} displays an alternate sign. Similarly, the Hall effect with the carrier flux driven by the temperature gradient predominates the Nernst coefficient when the chemical potential near the edge of the band lies below the LL. So S_{xy} is positive. Binding this with that in the electron side leads to a maximum of S_{xy} in the vicinity of the lowest LL. Experimentally, S_{xx} changes the sign from a dip to a peak with increasing μ around $\mu=0$. This discrepancy with our results is related to the lower ρ_{xx} value when μ is at the $n=0$ LL, which is also observed in other theoretical calculations by different methods.[44,45] Apart from this, the Seebeck coefficent S_{xx} and the Nernst coefficient S_{xy} are in good agreement with the experimental results.[15–17]

4.2.3. Thermal conductivities κ_{xx} and κ_{xy}

Figures 1(c) and 2(c) show the thermal conductivities as a function of chemical potential μ for $n\geq 0$ LL. The longitudinal component of thermal conductivity κ_{xx} is symmetric while the transverse component κ_{xy} is antisymmetric with respect to $\mu=0$. κ_{xx} shows a peak and κ_{xy} jumps to a new plateau when the chemical potential equals $\varepsilon_n=\mathrm{sgn}(n)\hbar\omega\sqrt{|n|}$. These behaviors are similar to those for the conductivities (resistivities). However, the peaks of κ_{xx} at those higher LLs split into two peaks which also have been shown in Ref. [47] and these split double peaks smear to one peak with increasing impurity. In addition, the transverse thermal conductivity exhibits a sign reversing behavior when the chemical potential skims over the zeroth LL as shown in Fig. 2(c). The sign reversing in κ_{xy} implies the effects of thermally excited electrons and holes for the zeroth LL state. The thermal conductivity contributions arising from electrons and holes are not simply additive, but in combination they give rise to an additional contribution known as the bipolar effect. In order to check the validity of the Wiedemann–Franz law, the thermal conductivity calculated by $\kappa_{xx}=L_0\sigma_{xx}T$ (where $L_0=\pi^2k_B^2/(3e^2)$) is shown in Fig. 3 for comparison with the numerical results. We see that at the central region of the LL, the Wiedemann–Franz law is violated. As shown in Fig. 3(b), because of the split double-peak structure of κ_{xx} and the non-constant space between nearest LLs, the peaks of the nearest LL merge into one peak when $n>6$, which is the origin of the out-of-phase oscillations with electrical conductivity in Ref. [43], even though the double peaks are clear when $n<6$. At low temperatures, the breadth of the LLs is narrow and the double peak structure is still clear as shown in Fig. 3(a). It is found that the enhancement of impurity scattering results in enhanced κ_{xx} and suppressed κ_{xy} as shown in Fig. 1(c). This double-peak structure of longitudinal thermal conductivity in high LLs and the anomalous jump

at the zeroth LL with a sign reversal in the transverse thermal conductivity have not yet been observed experimentally.

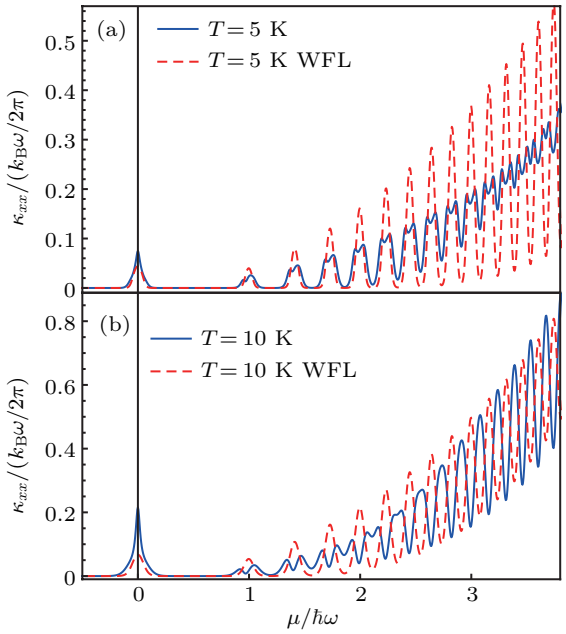


Fig. 3. (color online) The thermal conductivity κ_{xx} as a function of μ with $V = 0.001$ at (a) $T = 5$ K and (b) $T = 10$ K. The results calculated from the Wiedemann–Franz law by conductivity σ_{xx} are labeled by WFL in the legends.

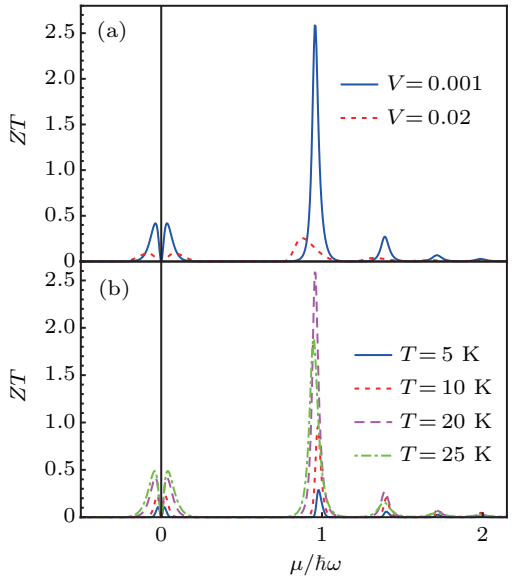


Fig. 4. (color online) The thermoelectric figure of merit as a function of μ (a) at $T = 20$ K with different V and (b) with $V = 0.001$ at different temperatures.

From the thermal and electrical transport coefficients, the thermoelectric figure of merit ZT is calculated and shown in Fig. 4. ZT exhibits a resonant like structure. The magnetically quantized graphene is a very good thermoelectric material when the chemical potential is pinned to the first LLs. This excellent ZT can be the basis for expanding the thermoelectrical application of graphene.[66,67] For practical applications with sufficient power output, graphene with a high carrier concentration is required. This would require a large magnetic field to locate the chemical potential in the first LL. A tradeoff between efficiency ZT and power needs to be considered to determine the optimal condition.

5. Summary

We have calculated the charge and thermal transport coefficients in magnetically quantized graphene in the presence of intra-valley impurity scattering. The Green's function and the self-energy are calculated in SCBA. A detailed investigation of the electrical and thermal properties of graphene in a magnetic field is performed by means of the Kubo–Středa formula in the presence of impurity scattering and thermal broadening. The results agree with the experimental ones qualitatively. The features of Seebeck coefficient and the transverse thermal conductivity at the zeroth LL are discussed and are associated with the intensity of impurity scattering. The sign reversal in the Seebeck coefficient and the transverse thermal conductivity imply the effects of thermally excited electrons and holes for the zeroth LL state. The impurity scattering may result in a bipolar effect from these thermally excited electrons and holes. Finally, our results of the thermoelectric figure of merit suggest that an external strong magnetic field could be used to effectively enhance the ZT.

References

[1] Novoselov K S, Geim A K, Morozov S V, Jiang D, Zhang Y, Dubonos S V, Grigorieva I V and Firsov A A 2004 *Science* **306** 666
[2] Novoselov K S, Geim A K, Morozov S V, Jiang D, Katsnelson M I, Dubonos S V, Grigorieva I V and Firsov A A 2005 *Nature* **438** 197
[3] Katsnelson M I, Novoselov K S and Geim A K 2006 *Nat. Phys.* **2** 620
[4] Neto A H C, Guinea F, Peres N M R, Novoselov K S and Geim A K 2009 *Rev. Mod. Phys.* **81** 109
[5] Sarma S D, Adam S, Hwang E H and Rossi E 2011 *Rev. Mod. Phys.* **83** 407
[6] Zhang Y, Tan Y W, Stormer H L and Kim P 2005 *Nature* **438** 201
[7] Zhang Y 2006 *Phys. Rev. Lett.* **96** 136806
[8] Zhang Z, Zhang Y, Stormer H L and Kim P 2007 *Phys. Rev. Lett.* **99** 106802
[9] Abanin D A, Novoselov K S, Zeilter U, Lee P A, Geim A K and Levitov L S 2007 *Phys. Rev. Lett.* **98** 196806
[10] Checkelsky J G, Li L and Ong N P 2008 *Phys. Rev. Lett.* **100** 206801
[11] Checkelsky J G, Li L and Ong N P 2009 *Phys. Rev. B* **79** 115434
[12] Giesbers A J M 2009 *Phys. Rev. B* **80** 201403(R)
[13] Bolotin K I, Ghahari F, Shulman M D, Stormer H L and Kim P 2009 *Nature* **462** 196
[14] Du X, Skachko I, Duerr F, Luican A and Andrei E Y 2009 *Nature* **462** 192
[15] Wei P, Bao W, Pu Y, Lau C N and Shi J 2009 *Phys. Rev. Lett.* **102** 166808
[16] Zuev Y M, Chang W and Kim P 2009 *Phys. Rev. Lett.* **102** 096807
[17] Checkelsky J G and Ong N P 2009 *Phys. Rev. B* **80** 081413(R)
[18] Liu X, Wang D, Wei P, Zhu L and Shi J 2012 *Phys. Rev. B* **86** 155414
[19] Nam Y, Sun J, Lindvall N, Yang S J, Park C R, Park Y W and Yurgens A 2014 *Appl. Phys. Lett.* **104** 021902
[20] Wang D and Shi J 2011 *Phys. Rev. B* **83** 113403
[21] Ghahari F, Xie H-Y, Taniguchi T, Watanabe K, Foster M S and Kim P 2016 *Phys. Rev. Lett.* **116** 136802
[22] Xu Y, Li Z and Duan W 2014 *Small* **10** 2182
[23] Sadeghi H, Sangtarash S and Lambert C J 2015 *Beilstein J. Nanotechnol.* **6** 1176

[24] Zheng H, Liu H J, Tan X J, Lv H Y, Pan L, Shi J and Tang X F 2012 *Appl. Phys. Lett.* **100** 093104
[25] Olaya D, Morales M H, Gómez D, Uribe O A C, Juang Z Y and Hernández Y 2018 *2D Mater.* **5** 011004
[26] Yadav S, Chaudhary S and Pandya D K 2018 *Ceram. Int.* **44** 10628
[27] Cheng X and Sun G Y 2017 *Physica E* **87** 84
[28] Nguyen M C, Nguyen V H, Nguyen H V, Martin J S and Dollfus P 2015 *Physica E* **73** 207
[29] Vishkayi S I and Soleimani H R 2015 *Physica E* **74** 363
[30] Patil U and Muralidharan B 2017 *Physica E* **85** 27
[31] D'Souza R and Mukherjee S 2016 *Physica E* **81** 96
[32] Rodriguez S T, Grosu I, Crisan M and Tifrea I 2018 *Physica E* **96** 1
[33] Valdovinos S M, Rivera J M, Cabrera N E M and Vargas I R 2018 *Physica E* **101** 188
[34] Tran V-T, Martin J S, Dollfus P and Volz S 2017 *Sci Rep* **7** 2313
[35] Anno Y, Imakita Y, Takei K, Akita S and Arie T 2017 *2D Mater.* **4** 025019
[36] Zberecki K, Swikowicz R, Wierzbicki M and Barnas J 2016 *Phys. Chem. Chem. Phys.* **18** 18246
[37] Kolesnikov D V, Lobanov D A and Osipov V A 2016 *Solid State Commun.* **248** 83
[38] Kim J Y and Grossman J C 2015 *Nano Lett.* **15** 2830
[39] Nam S G, Ki D K and Lee H J 2010 *Phys. Rev. B* **82** 245416
[40] Wang C R, Lu W S and Lee W L 2010 *Phys. Rev. B* **82** 121406
[41] Zhu Z W, Yang H, Fauqu B, Kopelevich Y and Behnia K 2010 *Nat. Phys.* **6** 26
[42] Gusynin V P and Sharapov S G 2005 *Phys. Rev. B* **71** 125124
[43] Dóra B and Thalmeier P 2007 *Phys. Rev. B* **76** 035402
[44] Zhu L, Ma R, Sheng L, Liu M and Sheng D N 2010 *Phys. Rev. Lett.* **104** 076804
[45] Chao S P and Aji V 2011 *Phys. Rev. B* **84** 155430
[46] Ugarte V, Aji V and Varma C M 2011 *Phys. Rev. B* **84** 165429
[47] Nasir R and Sabeeh K 2011 *J. Phys: Condens. Matter* **23** 375301
[48] Proskurin I and Ogata M 2013 *J. Phys. Soc. Jpn.* **82** 063712
[49] Xing Y, Sun Q F and Wang J 2009 *Phys. Rev. B* **80** 235411
[50] Wei M M, Zhang Y T, Guo A M, Liu J J, Xing Y and Sun Q F 2016 *Phys. Rev. B* **93** 245432
[51] Saito K, Nakamura J and Natori A 2007 *Phys. Rev. B* **76** 115409
[52] Yiğen S and Champagne A R 2014 *Nano Lett.* **14** 289
[53] Crossno J 2016 *Science* **351** 1058
[54] Ajiki H and Ando T 1993 *J. Phys. Soc. Jpn.* **62** 1255
[55] Ajiki H and Ando T 1996 *J. Phys. Soc. Jpn.* **65** 505
[56] Ando T and Nakanishi T 1998 *J. Phys. Soc. Jpn.* **67** 1704
[57] Ando T 2000 *Semicond. Sci. Technol.* **15** R13
[58] Ando T 2005 *J. Phys. Soc. Jpn.* **74** 777
[59] Shon N H and Ando T 1998 *J. Phys. Soc. Jpn.* **67** 2421
[60] Zheng Y and Ando T 2002 *Phys. Rev. B* **65** 245420
[61] Smreka L and Středa P 1977 *J. Phys.: Solide State Phys. C* **10** 2153
[62] Luttinger J M 1964 *Phys. Rev.* **135** A1505
[63] Jonson M and Girvin S M 1984 *Phys. Rev. B* **29** 1939
[64] Středa P 1983 *J. Phys. C* **16** L369
[65] Oji H and Středa P 1985 *Phys. Rev. B* **31** 7291
[66] Vining C B 2009 *Nat. Mater.* **8** 83
[67] Tritt T M 2011 *Annu. Rev. Mater. Res.* **41** 433